Applied Catalysis B: Environmental 168-169 (2015) 33–41

Contents lists available at ScienceDirect

Applied Catalysis B: Environmental

journal homepage: www.elsevier.com/locate/apcatb

Carbon monoxide and ethanol oxidation on PtSn supported catalysts: Effect of the nature of the carbon support and Pt:Sn composition

Jaime Asgardi[a], Juan Carlos Calderón[a], Francisco Alcaide[b], Amaia Querejeta[b], Laura Calvillo[c], Mª Jesús Lázaro[c], Gonzalo García[a], Elena Pastor[a,*]

[a] Departamento de Química Física, Instituto de Materiales y Nanotecnología, Universidad de La Laguna, Avda. Astrofísico Francisco Sánchez s/n, 38071 La Laguna, Santa Cruz de Tenerife, Spain
[b] División de Energía, IK4-CIDETEC, P° Miramón, 196, 20009 San Sebastián, Spain
[c] Instituto de Carboquímica, CSIC, Miguel Luesma Castán 4, 50018 Zaragoza, Spain

ARTICLE INFO

Article history:
Received 6 September 2014
Received in revised form
24 November 2014
Accepted 1 December 2014
Available online 3 December 2014

Keywords:
Ethanol electrooxidation
PtSn electrocatalysts
Carbon nanofibers
Direct ethanol fuel cell
Catalyst support

ABSTRACT

This paper presents the behavior of 20 wt.% PtSn supported catalysts as anodes for direct ethanol fuel cell (DEFC), which is fed with an aqueous ethanol solution. PtSn nanoparticles with different Pt:Sn ratios (1:1 and 3:1) were supported on carbon black and carbon nanofibers. Physicochemical characterization showed high particle dispersion onto the carbon supports and similar particle size (around 4.0 nm). XRD analysis indicated the presence of SnO_2 and similar lattice parameter for PtSn (1:1) to those of pure Pt_3Sn_1. Prepared catalysts were electrochemically studied in acidic medium by carbon monoxide (CO) stripping voltammetry, cyclic voltammetry, lineal sweep voltammetry and chronoamperometry in three-electrode cell experiments. In addition, cell voltage vs. current density curves were recorded in a DEFC. It was found that PtSn anodes exhibit good activity toward ethanol electrooxidation in half-cell experiments under fuel cell relevant conditions. Specifically, PtSn supported catalysts on carbon black showed higher catalytic activity compared to those supported on carbon nanofibers. The low activity for ethanol adsorption/deprotonation and C—C cleavage appear as the main causes for the low performance for ethanol oxidation reaction on catalysts supported on carbon nanofibers. A similar behavior was observed in single fuel cell experiments.

1. Introduction

Direct liquid ethanol fuel cells (DEFC) are promising energy sources for portable applications. Ethanol has several advantages, such as its high energy density (8.03 kWh kg^{-1}) compared to that of methanol (6.1 kWh kg^{-1}), in addition to its higher solubility in liquid electrolytes, availability at low cost, easier handling, transport and storage [1]. Furthermore, ethanol is a non-toxic fuel and it can be produced in large quantities by the fermentation process of sugar-containing biomass or agricultural products. Although the feasibility of DEFC has been established by single cell experiments [2–6], the commercial development of these systems is still far away, and further progresses are necessary to improve their performance and efficiency [7], due to the limitations related to the ethanol electrooxidation reaction. It is well known that the main oxidation products are soluble acetic acid and acetaldehyde, instead the complete oxidation to CO_2 [8–11]. Ethanol electrooxidation at low temperature (<100 °C) on PdSn based catalysts yields a products mixture with the following composition (ordered according to their concentration): acetic acid > acetaldehyde ≫ CO_2 [4]. The activation for the C—C bond of ethanol appears as an important challenge for its oxidation to CO_2 that is not necessary for formic acid or methanol oxidation reactions. Consequently, under electrocatalytic conditions, the current density produced via the total oxidation to CO_2 (as the result of C—C bond activation), is only a few percent. Most of the current is produced from the ethanol partial oxidation to acetaldehyde or acetic acid [12]. The formation of CO_2, CH_3CHO and CH_3COOH has been confirmed by spectroelectrochemical and chromatographic measurements [13].

Recently, considerable effort has been directed toward the development of high catalytic activity anodes for ethanol electrooxidation (EOR). The electrocatalyst optimization has involved two routes: (i) the development of new catalysts syntheses with attention to alloy composition, that is, the enhancement of the platinum activity by using binary and ternary electrocatalysts [14], like

* Corresponding author. Tel.: +34 922 318071; fax: +34 922 318002.
E-mail address: epastor@ull.edu.es (E. Pastor).

http://dx.doi.org/10.1016/j.apcatb.2014.12.003
0926-3373/

Pt–X where X = Ru, Sn, Rh, Mo [15–17], Pt–Sn–Ru, Pt–Sn–W and Pt–Rh–SnO_2 [18–20] among others; and (ii) the development of new carbon supports of high electric conductivity with a high accessible surface area to allow a good dispersion of metal nanoparticles.

Traditionally, catalyst supports have received less attention, despite the catalyst–support interaction strongly influences the physicochemical and electrochemical properties of the catalysts and, as a consequence, its performance under fuel cell operation [21,22]. It is usually suggested that the use of carbon materials with an ordered structure and high electrical conductivity improves the fuel cell performance, and because of this, many research groups have recently made efforts to synthesize and use different novel carbon supports such as nanotubes [23–27], nanofibers [28,29], carbon microspheres [30,31], hard carbon spherules [32], carbon aerogels and xerogels [33,34], and mesoporous carbons for fuel cell applications [35]. In particular, carbon nanofibers (CNF) have been extensively studied as catalyst support for the electrooxidation of alcohols, mainly for their high resistance to corrosion [36–38] and their high electrical conductivity that make them good candidates to replace the commercial Vulcan XC-72R support. In this context, recently was observed that catalysts supported on CNF shown an enhanced activity toward CO and alcohol oxidation reactions, respect to commercial catalyst supported on carbon back [36]. In addition, both their structural properties and surface chemistry can be easily tailored to obtain a material with the desired properties [29,39].

Another important factor is the metal–support interaction that plays an important role in catalysis, since this interaction determines the physicochemical and electrochemical properties of the materials. Regarding the physicochemical properties, the size and morphology of the metal particles depend on the nature of the support. High crystalline grade of the support (graphitic character) induces the formation of small metal particles with high crystallinity, which is associated with a strong metal–carbon interaction. On the other side, amorphous carbon support produces spherical metal particles with high size and mass density. The last features are related with a weak metal–carbon interaction [40].

Regarding to the electrochemical properties, the carbon support changes the electronic structure of the supported metal particles and consequently the electronic structure of the catalyst (metal–support interaction). Thus, it is expected that different carbon materials change the electronic structure of the catalysts in a different way. The metal–support interaction may affect the electron transfer from metal particles to the carbon support during the electrochemical reactions, thus changing the catalyst performance in the fuel cell [41]. In addition, the metal–support interaction can be attained through the oxygenated groups of the carbon surface, which play an important role in the electron transfer from metal particles to the support.

An efficient catalyst for ethanol electrooxidation should have a suitable surface for alcohol adsorption and a high tolerance toward CO and other intermediate ad-species during alcohol electrooxidation, and the ability to cleavage the C—C bond of the ethanol molecule at operating conditions compatible with the other fuel cell components. As it is pointed above, Pt has been modified with more oxophilic metals, like Ru, Sn, Rh, Mo, to improve its CO tolerance, because these atoms promote the formation of oxygenated species (e.g. OH_{ad}) at more negative potentials than Pt. Among these materials, Pt–Sn based electrocatalysts have presented the best performance during the ethanol oxidation in acidic media [2–4,42]. In Ref. [4], the best results were obtained using a Pt:Sn atomic ratio of 83:17, meanwhile in Ref. [43] the same authors suggested that the optimum Sn composition in the catalyst was in the range of 10–20% (atomic ratio). In fact, the optimum atomic composition of Pt–Sn has not yet been well established. The last is consequence of different factors, though catalyst preparation methods appear as the most important issue [44–46]. In this sense, the choice of the catalyst synthesis will provide diverse Pt–Sn ratios (in the bulk and on the surface) and alloy degree with a tremendous effect of the catalyst performance [15].

In this paper we report the synthesis and the electrochemical behavior of Pt–Sn nanoparticles supported on carbon black and carbon nanofibers toward ethanol electrooxidation in half-cell and single direct ethanol fuel cell (DEFC), under operating conditions used in practical fuel cells, in addition to their suitability for their use as anodic electrocatalysts in these systems.

2. Experimental

2.1. Synthesis of catalysts and physical characterization

Carbon nanofibers (CNFs) have been prepared using the methodology described in our earlier works [47]. Briefly, the CNFs were grown by decomposition of a methane flow on a Ni:Cu:Al catalyst (atomic ratio = 78:6:16) at 700 °C for 10 h. Then, both the CNFs and commercial carbon Vulcan XC-72R were treated in a HNO_3–H_2SO_4 1:1 (v/v) mixture for 0.5 h at room temperature during 30 min to create surface oxygenated groups. The original prepared CNF contains around 8 wt.% of metals, which act as catalyst for the carbon nanofibers production process. After that, the catalyst is eliminated during the acid treatment used to create oxygenated groups at the CNF surface.

N_2 adsorption–desorption isotherms of the carbon supports were measured at −196 °C using a Micromeritics ASAP 2020. The total surface area was calculated from BET (Brunauer, Emmett and Teller) equation and the total pore volume was determined using the single point method at $P/P_0 = 0.99$. Pore size distribution (PSD) curves were obtained from the analysis of the desorption branch of the N_2 isotherm using the BJH (Barrett, Joyner and Halenda) method.

The surface chemistry of functionalized CNFs was analyzed by temperature programmed desorption (TPD). The experiments were performed in a Micromeritics Pulse Chemisorb 2700 instrument, under a flow of helium and using a heating rate of 10 °C min^{-1} from 150 °C up to 1050 °C. The amounts of CO and CO_2 desorbed from the samples were analyzed by gas chromatography.

The carbon Vulcan XC-72R and CNF supported electrocatalysts (Pt_1Sn_1/C, Pt_3Sn_1/C, Pt_1Sn_1/CNF, Pt_3Sn_1/CNF) were prepared by the formic acid method (FAM) [48]. Appropriate amounts of metal precursor (H_2PtCl_6 and $SnSO_4$, Sigma–Aldrich) were used to obtain nominal metal loading of 20 wt.% on the support material.

X-ray diffractograms (XRD) of the electrocatalysts were obtained with an universal diffractometer Carl Zeiss-Jena, URD-6, operating with CuKα radiation ($\lambda = 0.15406$ nm) generated at 40 kV and 20 mA. Scans were done at 38 min^{-1} for 2θ values between 20° and 100°. In order to estimate the particle size from XRD, the Scherrer equation was used [49]. In order to improve the fitting of the peak, diffractograms for specific 2θ values ranges were recorded at 0.028 min^{-1}. The lattice parameters were obtained by refining the unit cell dimensions applying the least squares method [50].

Transmission electron microscope (TEM) micrographs for the PtSn electrocatalysts were obtained using a JEOL-2000 FXII microscope equipped with a LaB6 gun. The samples were grounded, dispersed in ethanol and a drop of solution was then deposited on a copper grid.

The atomic ratios for Pt:Sn were determined by energy dispersive X-ray analysis (EDX) coupled to the scanning electron microscopy LEO Mod. 440, with a silicon detector and Be window, applying 20 keV.

2.2. Electrode preparation and electrochemical characterization

All measurements were carried out in a three-electrode cell at room temperature (25 °C) controlled by an Autolab PGSTAT302N potentiostat–galvanostat. A carbon row was used as a counter electrode, while the reference electrode was a reversible hydrogen electrode (RHE) in the supporting electrolyte (0.5 M H_2SO_4, Merck, p.a.). All potentials are referred to this electrode. The working electrode consisted in a catalyst suspension (20 μL) dried onto the glassy carbon disk under Ar atmosphere. The suspension was prepared by stirring 4 mg of catalyst with 30 μL of Nafion® (5%, Sigma–Aldrich) and 1 mL of water (Milli-Q, Millipore).

The experiments were carried out in 0.5 M sulphuric acid (Merck p.a.) solutions prepared in Milli-Q water (Millipore). First, the electrolyte was saturated with pure argon (N50, Air Liquide) and subsequently ethanol (Merck) was added until a final concentration of 2 M was reached.

A previous electrochemical activation step was realized before the electrochemical measurements. With this end, the working electrode was subjected to 20 potentiodynamic cycles between 0.05 and 1.0 V at 0.2 V s^{-1} in the supporting electrolyte. After that, stable and reproducible cyclic voltammograms were recorded at 0.02 V s^{-1} in the supporting electrolyte.

Current transient curves in the presence of ethanol were obtained by stepping the potential from 0.05 V (potential in which ethanol is not oxidized) to 0.45 or 0.50 V (typical potential values for the anode of a direct ethanol fuel cell in the operation mode). Regarding to the potentiodynamic experiments, the working electrode was introduced into the electrochemical cell containing the alcohol solution at controlled potential of 0.05 V and subsequently cyclic voltammograms were recorded at 0.02 V s^{-1}.

CO stripping voltammograms were obtained after bubbling CO gas (N47, Air Liquide) in the cell for 10 min at 0.07 V, followed by electrolyte exchange and argon purging to remove the excess of CO. These experiments were used to study the CO tolerance and to obtain the electrochemical area (EA) that is used for current normalization. EA were determined from the integration of the current involved in the oxidation of a CO monolayer taking into account that CO adsorbs only on Pt and assuming a charge of 420 μC cm^{-2}.

2.3. Membrane electrode assembly preparation and electrochemical characterization

Membrane electrode assemblies (MEAs) of geometrical area of 5 cm^2 were prepared using the hot press method [51]. 20 wt.% Pt–Sn/C and commercial 40 wt.% Pt on Vulcan XC-72R (Premetek Co.) catalysts were used for the anode and the cathode, respectively. Appropriate amounts of catalyst powders and 5 wt.% Nafion® ionomer dispersion (Aldrich), were ultrasonically mixed in a mixture of isopropyl alcohol and ultrapure water to form a homogeneous catalyst ink. Then, the ink was sprayed onto a diffusion layer by an air-brush gun fed with pure nitrogen (99.999%, from Praxair). The anode diffusion layer was a hydrophobized Toray carbon paper covered with a microporous layer made of Vulcan XC-72R and polytetrafluoroethylene. The cathode gas diffusion layer was ELAT SS (BASF Fuel Cell, Inc.). The metal loading was 2.0 mg cm^{-2} in both electrodes. Nafion 115 membranes were cleaned and converted into the acid form by boiling in 3% H_2O_2 for 1 h, then in 0.5 M H_2SO_4 for 2 h, and finally in ultrapure water for 2 h with the water being changed every 30 min. The cleaned membrane was stored in ultrapure water and dried before use. Each MEA was assembled by hot-pressing the anode and cathode on either side of the pretreated membrane at 50 bar, 130 °C for 180 s.

Single cell experiments were performed placing a MEA in a commercial fuel cell hardware FCT 5SCH (Fuel Cell Technologies, Inc.), which was assembled using an uniform torque of 5 Nm. Single cells were operated with a 2.0 mol dm^{-3} aqueous ethanol solution pumped through the anode compartment at 1.5 mL min^{-1} and zero back-pressure from a reservoir at 40–90 °C, and with humidified O_2 from cylinders passed through the cathode compartment at 50 standard cubic centimeters per minute (sccm) and zero back-pressure. The MEA performance was evaluated by measuring the current–voltage curves (potentiostatic polarization plots at steady-state condition, in our case 5 min per point) using a fuel cell test station built up in our laboratory. Previously, the MEA was conditioned circulating deionized water at 40–70 °C through the anode and cathode compartments for 12 h. After that, polarization curves were registered until they stabilized.

3. Results and discussion

3.1. Structural characterization of catalysts

Textural properties of the untreated and functionalized carbon supports are given in Table 1, all obtained from N_2-physisorption measurements. It is observed that the specific surface area and total pore volume are only slightly modified by the chemical treatment. CNFs show a specific surface area and pore volume around 100 m^2/g and 0.22 m^3 g^{-1}, respectively, and a mesoporous structure (mesoporosity higher than 90% in surface and 99% in volume), whereas Vulcan XC-72R has a specific surface area of 218 m^2/g and a total pore volume of 0.40–0.60 m^3 g^{-1}, being the 30% of its area belonging to the micropores. Thus, reactants and products can diffuse faster into the CNFs structure in comparison to Vulcan-based materials, and consequently a better performance of CNFs-based catalysts is expected.

The functionalization treatment on the CNFs and carbon Vulcan led to a considerable increase in the amount of surface oxygen groups. In Table 2 the total amounts of CO_2 and CO desorbed from the untreated and functionalized materials are summarized. It is to be noted that the untreated CNFs presents a certain amount of oxygen groups and after functionalization the oxygen content is about two times higher. In the case of Vulcan XC-72R, initially only small amounts of quinone groups are present on the surface and after chemistry treatment the number of oxygen containing groups is increased around seven times. From TPD profiles (not shown) it was found that the highest contribution to oxygenated surface groups comes from quinone and phenol groups for CNFs and phenol and carboxyl groups for the commercial carbon black.

According to these results, it can be concluded that the chemical treatment applied allows the increase of the amount of oxygenated surface groups to facilitate metal particle anchoring, maintaining the textural properties of the carbonaceous material. Then, functionalized materials have been chosen for the preparation of the PtSn/C and PtSn/CNF catalysts.

The physicochemical parameters and the electrochemical surface area (ECSA) of Pt_1Sn_1/C, Pt_3Sn_1/C, Pt_1Sn_1/CNF, Pt_3Sn_1/CNF catalysts based on EDX, XRD and CO stripping analysis are compiled in Table 3. X-ray diffractograms of all synthesized catalysts and a commercial 20 wt% Pt/C (ETEK) material are given in Fig. 1. XRD patterns clearly show the five main characteristic peaks of the face centered cubic (fcc) crystalline Pt, namely, the planes (1 1 1), (2 0 0), (2 2 0), (3 1 1), and (2 2 2). Additionally, it is observed the plane (0 0 2) at 24.5° associated to graphitic carbon. These five diffraction peaks at Pt–Sn catalysts are slightly shifted to lower angles with respect to the corresponding peaks in Pt/C, indicating an expansion of the lattice and alloy formation. Noticeable is the higher lattice expansion with the Sn loading into the material. In this context, Pt and Sn can produce solid alloys at almost any stoichiometry leading to fcc phases when the atomic percentages of Sn is lower than 25%, but to hcp phases for Sn atomic

Table 1
Textural properties of carbon supports.

Sample	S_{BET} (m^2/g)	V_{Total} (cm^3/g)	$V_{Micropore}$ (cm^3/g)	$V_{Mesopore}$ (cm^3/g)	$S_{Micropore}$ (m^2/g)	$S_{Mesopore}$ (m^2/g)
XC-72R	218	0.41	0.03	0.38	65	153
XC-72R NSTa0,5	218	0.58	0.04	0.54	65	153
CNF	95.7	0.23	0.001	0.23	4.0	91.7
CNF NSTa0,5	102.7	0.22	0.003	0.22	7.6	95.1

Table 2
CO_2 and CO desorbed in TPD experiments from oxygen surface groups in the carbon supports.

Sample	CO_2 peak area (μmol/g)		CO peak area (μmol/g)			$CO + CO_2$ (μmol/g)	CO/CO_2
	Carboxyl	Lactone	Anhydride	Phenol	Carbonyl quinone		
XC-72R	0	0	0	0	317	317	–
XC-72R NSTa0,5	464	231	55	1144	140	2089	1.80
CNF	11	20	0	68	153	252	6.90
CNF NSTa0,5	64	1031	2	139	235	543	2.20

Table 3
Physicochemical parameters of the catalysts synthesized.

Catalyst	Metal loading (wt%)	Atomic ratio (Pt:Sn)	Particle size (nm)	Lattice parameter (fcc) (A)	Electroactive surface area (cm^2)
Pt_1Sn_1/C	19	53:47	3.6	3.972	9.40
Pt_1Sn_1/CNF	21	50:50	4.7	3.978	5.93
Pt_3Sn_1/C	19	73:27	4.1	3.935	10.42
Pt_3Sn_1/CNF	25	77:23	3.9	3.943	8.09

percentages higher 25% [2–4,42,43]. Since only fcc phases is observed at the X-ray diffractograms, the actual incorporation of Sn into the Pt network should be as high as 25 at.%. X-ray diffraction peaks at ca. 34° and 52°, which are associated to SnO_2 phases, support the last assumption. In this sense, higher intensity for the SnO_2 species is achieved at Pt_1Sn_1 than Pt_3Sn_1 materials, and the lattice parameter of the Pt_1Sn_1 samples is closer to that for pure Pt_3Sn_1 solid solution (4.001 A, JPCDS 00-035-1360]. These features indicate that Pt_1Sn_1 has higher amount of Pt_3Sn_1 crystallites with fcc phases and SnO_2 phases than the Pt_3Sn_1 sample. Consequently, Pt_1Sn_1 and Pt_3Sn_1 catalysts are composed mainly of Pt_3Sn_1 and Pt_3Sn_{1-x} ($0 < x < 1$) crystallite phases, respectively. In addition all the samples have a small but visible amount of SO_2 species.

On the other hand, XRD analyses reveal similar particle sizes for all catalysts (approx. 4.0 nm), which suggest an exclusive dependence of the particle size with the synthesis methodology in the present conditions. A regular distribution of the PtSn particles over the carbonaceous supports was proved from TEM micrographs (Fig. 2).

Finally, Pt:Sn ratio and metal loading from EDX remain similar to the nominal values (Table 3). However, metal loadings are slightly higher for catalysts with CNF as support, probably occasioned by the higher facilities for Pt anchoring to the CNF surface through the functional groups due to the lower microporosity of the support.

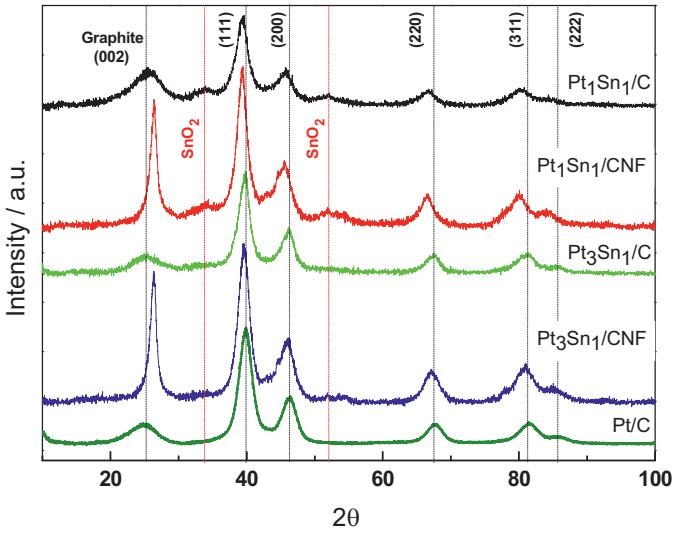

Fig. 1. X-ray diffraction patterns of carbon and carbon nanofibers supported electrocatalysts.

3.2. CO stripping voltammetry

The activities of the catalysts toward carbon monoxide electrooxidation provide insight about their tolerance toward CO poisoning, which is one of the most important issues concerning the alcohol electrooxidation in direct alcohol fuel cell anodes, as adsorbed CO (CO_{ad}) is the principal catalyst poison produced during alcohol oxidation. Then, CO_{ad} monolayer oxidation measurements ("CO stripping experiments") were performed at 0.02 V s^{-1} in sulphuric acid solution at room temperature. Moreover, the anodic charge obtained from the CO stripping measurements was used to achieve the electroactive surface area (ESA, Table 3) [52].

The resulting stripping voltammograms recorded on the different catalysts are shown in Fig. 3 (red curves), together with the subsequent voltammograms (black curves). It is observed that CO is completely removed after the first cycle voltammogram. Also, similar voltammetric profiles of both blank (not shown) and second voltammogram after CO stripping (black curves) are achieved. The last indicates an electrochemical stability of the catalysts under study in the potential range applied for these studies. Furthermore, all catalysts display some of the typical features observed at Pt/C catalysts [53]. In this sense, analyzing the black curves in Fig. 3, it is observed that the hydrogen adsorption/desorption potential region is less resolved for Pt_1Sn_1 than for Pt_3Sn_1 catalysts, due to their lower platinum content. Accordingly, hydrogen adsorption/desorption peaks on sites with (1 1 0) and (1 0 0) orientations are clearly observed at Pt_3Sn_1/CNF material.

Noticeable is the quasi absence of the characteristic double layer region related to Pt when Sn is introduced in the material. In fact, at potentials more positive than 0.40 V, an anodic current develops

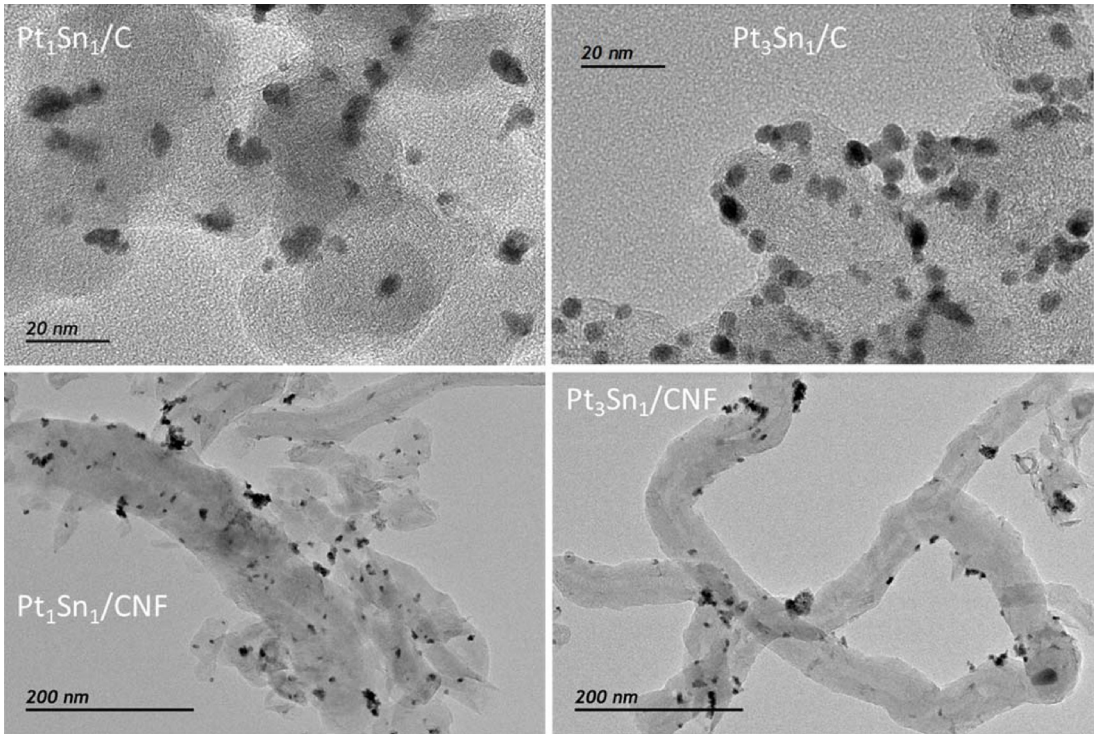

Fig. 2. TEM images of Pt_1Sn_1/C, Pt_3Sn_1/C, Pt_1Sn_1/CNF and Pt_3Sn_1/CNF catalysts.

during the positive going scan direction, which is associated with the catalyst surface oxidation. In this context, it has to be taken in mind that Pt nanoparticles supported on Vulcan presents the onset for surface oxidation at potentials higher than 0.70 V [53]. Therefore, the presence of Sn in the material produces an increment of the oxophilic behavior of the catalyst, i.e. water dissociation is facilitated with Sn insertion in the catalyst causing the shift of almost 0.30 V for the onset of surface oxidation. Furthermore, it is observed for all catalysts in Fig. 3 a redox pair with a common anodic peak at ca. 0.75 V. However, their cathodic counterpart depends on the catalyst support and the metallic atomic ratio. Thus, both carbon black supported catalysts develop a similar cathodic peak at ca. 0.55 V, which is located at more negative potentials than those observed for catalysts supported on CNF. This result indicates a higher degree of reversibility of the surface oxidation/reduction process for catalysts supported on CNF.

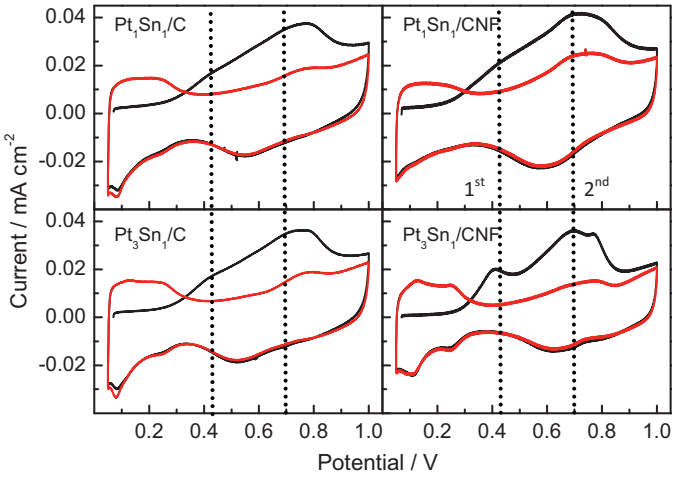

Fig. 3. CO stripping voltammetry (red curves) for Pt_1Sn_1/C (upper left panel), Pt_1Sn_1/CNF (upper right panel), Pt_3Sn_1/C (bottom left panel) and Pt_3Sn_1/CNF (bottom right panel) catalysts recorded in 0.5 M H_2SO_4 at 20 °C. ν = 20 mV s^{-1}. Admission potential: 0.070 V. Currents were normalized by the electrochemically active surface area obtained from CO stripping measurements. Black curves correspond to the second cycle after the CO stripping. (For interpretation of the references to color in this figure legend, the reader is referred to the web version of this article.)

Regarding CO removal (red curves in Fig. 3), the broad anodic current in the voltammograms is associated to surface sites with different catalytic activity toward CO oxidation. Additionally, very reactive sites are responsible for the oxidation currents around 0.40 V (a clear peak can be seen in the case of Pt_3Sn_1/CNF). However, not all CO is oxidized in this potential region, suggesting for all catalysts a restricted or slow CO surface diffusion toward these reactive sites. This effect can be caused by different factors, such as high CO adsorption energy, blocking effect by adsorbed sulphate species or geometric effects [54]. In this sense, the anodic pre-peak observed at Pt_3Sn_1/CNF resembles that of Pt-based catalyst with high density of defects (e.g. low coordinated sites) or particle agglomeration (e.g. grain boundary sites) [55].

On the other hand, an increment of the catalytic activity toward CO oxidation is observed with the presence of Sn compared with carbon supported Pt catalyst [56]. In fact, all the catalysts develop an onset potential for CO oxidation at potentials lower than 0.25 V that indicates the rise of CO tolerance with Sn introduction in the catalytic material. The onset potential for CO oxidation is similar for all catalysts but it slightly decreases in the order: Pt_3Sn_1/C ~ Pt_3Sn_1/CNF > Pt_1Sn_1/C > Pt_1Sn_1/CNF. This result agrees well with that reported by Lim and coworkers [57], pointing out that the onset potential for CO oxidation was very similar for different PtSn/C catalysts, irrespective of the Sn loading. However, we found a small but clear enhancement for the CO tolerance with the rise of Sn in the catalytic material, in agreement with the general consensus that Pt_3Sn_1 crystallite phase, which is the main phase at Pt_1Sn_1 catalysts, is the most active one for the CO oxidation reaction [58]. In this context, a catalyst support effect on the CO oxidation reaction can be discerned. Catalysts supported on CNF and carbon Vulcan XC-72R develop the main CO oxidation peak at ca. 0.70 and

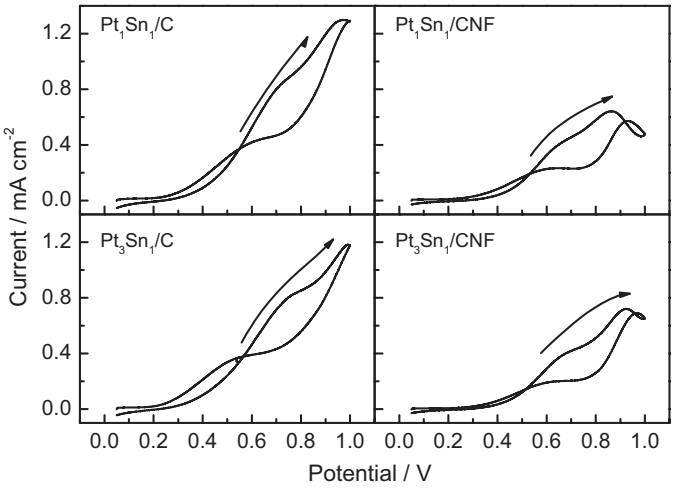

Fig. 4. Cyclic voltammograms for Pt_1Sn_1/C (upper left panel), Pt_1Sn_1/CNF (upper right panel), Pt_3Sn_1/C (bottom left panel) and Pt_3Sn_1/CNF (bottom right panel) electrodes recorded in 0.5 M H_2SO_4 + 2.0 M ethanol at 20 °C. ν = 20 mV s^{-1}. Currents were normalized by the electrochemically active surface area obtained from CO stripping measurements.

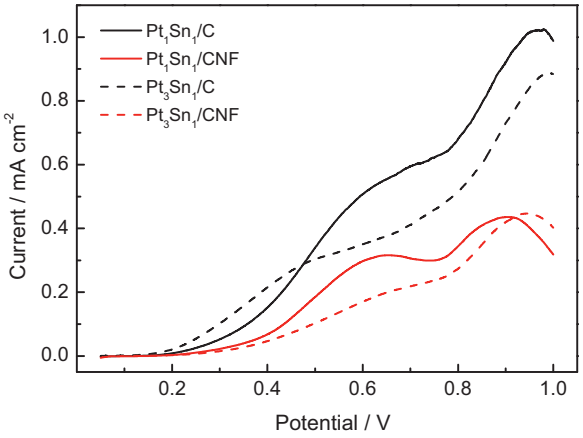

Fig. 5. Linear sweep voltammograms for Pt_1Sn_1/C (black solid line), Pt_1Sn_1/CNF (red solid line), Pt_3Sn_1/C (black dash line) and Pt_3Sn_1/CNF (red dash line) electrodes in 0.5 M H_2SO_4 + 2.0 M ethanol at 20 °C. ν = 2.0 mV s^{-1}. Currents were normalized by the electrochemically active surface area obtained from CO stripping measurements. (For interpretation of the references to color in this figure legend, the reader is referred to the web version of this article.)

0.75 V, respectively. Therefore, taking into account the onset and peak potentials and the anodic charge developed at low overpotentials, the tolerance to CO poisoning follows the tentative order: Pt_1Sn_1/CNF > Pt_1Sn_1/C ~ Pt_3Sn_1/CNF > Pt_3Sn_1/C. It seems that the decrease in the microporosity or the type/distribution of surface oxygenated groups, and the amount of both superficial species Pt_3Sn_1 crystallite and SnO_2 phases, favor the oxidation of CO at the CNFs. According to these observations, it can be concluded that both the metallic phase/s and catalyst support are important factors for the catalytic activity.

3.3. Ethanol electrooxidation under potentiodynamic conditions

The ethanol electrooxidation reaction on Vulcan XC-72R and CNF supported PtSn catalysts was study by cyclic voltammetry (CV) in 0.5 M H_2SO_4 + 2.0 M CH_3CH_2OH solution at room temperature. The experiment consists in the introduction of the working electrode into the solution at controlled potential of 0.05 V, for recording CVs up to 1.0 V to avoid tin dissolution, at scan rate of 0.020 V s^{-1}. Fig. 4 shows the stable CVs for all catalysts in acidic media (which corresponds to the third CV in all cases). In these plots the currents are normalized using the electroactive surface area determined by CO_{ad} stripping experiments.

Current density values in the hydrogen adsorption/desorption region (E < 0.4 V) are very small in the presence of ethanol, probably caused by alcohol adsorption on the electrocatalyst surface that inhibits hydrogen adsorption and other surface reactions. It is remarkable that the voltammetric profiles for carbon black and CNF supported materials are quite different. First of all, both catalysts supported on Vulcan XC-72R display higher current densities in all potential range studied, indicating that carbon Vulcan is the support that presents the best influence on the ethanol oxidation reaction. Probably for the EOR, the presence of a higher amount of surface oxygenated groups on the carbon support is the determining factor for a better activity. Secondly, the surface of the metallic particles supported on CNF oxidizes at lower potentials than those supported on Vulcan XC-72R. The latter is evident from the drop of the current after the main anodic peak, which is developed at more negative potentials on CNF supported catalysts. In this sense, it is well known that alcohol adsorption is inhibited on oxidized surfaces, and consequently, the anodic current decays as soon as oxide is formed [53].

This result is in agreement with previous CO stripping experiments (red curves in Fig. 3) in which catalysts supported on CNF develop the main anodic peak at lower potentials than those supported on carbon black, i.e. water dissociation is favored on CNF-based materials. Therefore, CO formation during ethanol oxidation reaction may not be the main cause for the low activity observed on CNF-based catalysts. In fact, low activity for ethanol adsorption/deprotonation and C—C cleavage appear as plausible causes for this behavior.

Regarding to the Pt:Sn atomic ratio, similar CVs and maxima current densities are observed for the potentiodynamic oxidation of ethanol in Fig. 4 with the rise of noble metal content and the Pt_3Sn_1 crystallite phase in the catalytic material. Therefore, catalysts with 1:1 Pt:Sn atomic ratio seem to present better performance to be used as anode in a real fuel cell in terms of cost. In this sense, Pt_1Sn_1/C appears to be the best material in good agreement with the results found in Refs. [59,60].

3.4. Ethanol electrooxidation under potentiostatic conditions

To study the catalyst activity under "long-term" fuel cell practical conditions, which is especially important when studying such self-poisoning reactions as ethanol electrooxidation, it was carried out tests at constant potentials during 15 min. In order to choice the most appropriate potentials, linear sweep voltammetry was performed at low scan rate (0.002 V s^{-1}) to achieve a quasi steady-state condition, and consequently, stationary currents. Fig. 5 shows the linear sweep voltammograms recorded for all catalysts at room temperature in 0.5 M H_2SO_4 + 2.0 M CH_3CH_2OH solution. The trend in catalytic activity for ethanol oxidation is similar to that recorded during the cyclic voltammetry experiments, i.e. Vulcan-based materials develop better performance than CNF-based catalysts toward ethanol oxidation. On the other hand, two anodic peaks are well resolved (especially on Pt_1Sn_1 catalysts) when the sweep rate is very low, which suggest two different operating reaction pathways that are mainly dependent on the Pt:Sn atomic ratio and the content of Pt_3Sn_1 phases of the material. An important difference respect to those results obtained from cyclic voltammetry is the change in activity at ca. 0.5 V for Vulcan-based materials. It is important to consider that this potential region is of main interest for DEFC applications. Accordingly, current transients experiments were performed at 0.45 and 0.55 V.

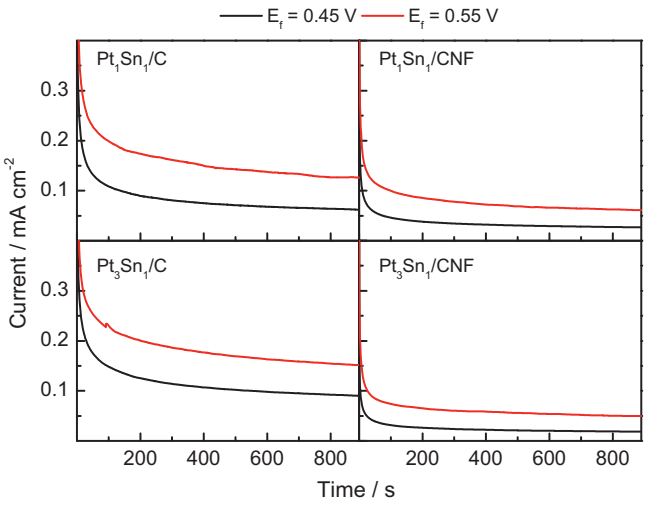

Fig. 6. Potentiostatic electrooxidation of ethanol on Pt_1Sn_1/C (upper left panel), Pt_1Sn_1/CNF (upper right panel), Pt_3Sn_1/C (bottom left panel) and Pt_3Sn_1/CNF (bottom right panel) electrodes recorded at (black solid line) 0.45 V and (red solid line) 0.55 V in 0.5 M H_2SO_4 + 2.0 M ethanol at 20 °C. Currents were normalized by the electrochemically active surface area obtained from CO stripping measurements. (For interpretation of the references to color in this figure legend, the reader is referred to the web version of this article.)

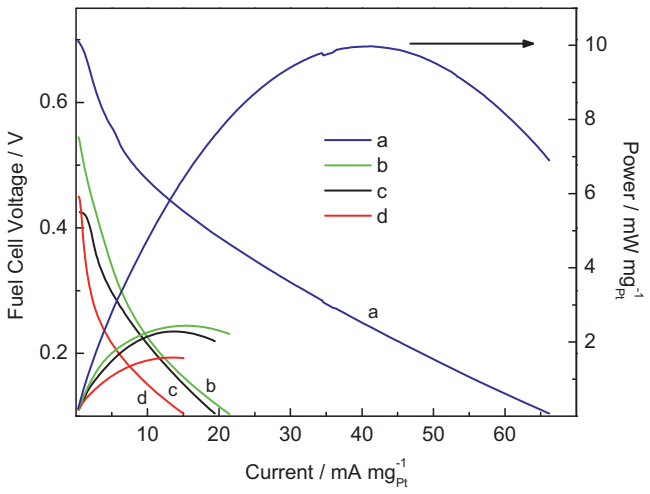

Fig. 7. Voltage vs. current and power vs. current curves for DEFC with (a) Pt_1Sn_1/C, (b) Pt_3Sn_1/C and (c) Pt_1Sn_1/CNF, and (d) Pt_3Sn_1/CNF catalyzed anodes operating at 70 °C, 2.0 M CH_3CH_2OH at 1.5 mL min^{-1}. Cathode: 2.0 mg_{Pt} cm^{-2} Pt/C catalyst, dry O_2 at 50 mL min^{-1}. Current and power normalized per mass of Pt in anodes.

Fig. 6 displays the current transients for all catalysts achieved during the EOR at 0.45 (black lines) and 0.55 V (red lines). In general, the curves featured a sharp decrease during the earlier minutes. Afterwards, the current diminishes much more slowly attaining a quasi-steady state. This behavior has been ascribed to the accumulation of adsorbed poisoning species, most likely CO_{ad} and $CH_{x,ad}$, on the catalyst surface during the ethanol electrooxidation [61]. However, as it was pointed out above, small contribution of the C—C cleavage is expected on the present catalysts.

Vulcan supported catalysts develop much better catalytic activity respect to CNF supported materials, which is in total agreement with cyclic (Fig. 4) and linear sweep voltammetry results (Fig. 5). Furthermore, the catalytic activity observed at the current transients decreases in the following order: Pt_3Sn_1/C > Pt_1Sn_1/C > Pt_1Sn_1/CNF > Pt_3Sn_1/CNF. However, it should be noticed that the differences in the stationary current densities between the 3:1 and 1:1 Pt:Sn materials are small.

3.5. Tests in single direct ethanol fuel cell (DEFC)

Even if voltammetric and current transient measurements are very useful to check the activity of an electrocatalyst, it is necessary to observe the response of the same material in a practical fuel cell, because the operating conditions such as temperature, pressure, and fuel flow-rates are capital to determine the real performance of a system.

Fig. 7 depicts the voltage and power vs. current curves obtained in the single DEFC operating with a 2 M aqueous ethanol solution at 70 °C and atmospheric pressure. The cathode feed was pure O_2, at atmospheric pressure, to maximize the activity of the cathode and thereby to minimize cathode effects on the relative activities of the cell. It is apparent that there were differences in the performance toward ethanol oxidation in terms of produced power for the different catalysts. The curves show that the open circuit voltage (OCV) ranged from 0.42 to 0.70 V. It is remarkable that the MEAs containing anodes with Vulcan as catalyst support develop higher OCVs than those with CNFs as catalyst support. Given that the manufacturing method of MEAs, and the membrane electrolyte was the same for all of them, it is suggested that the textural properties of catalyst support affect the properties of the catalyst layer/membrane interface, and then modify ethanol crossover through the membrane, and consequently the OCV [62]. The best performance was obtained when Pt_1Sn_1/C catalyst was used to prepare the anodes in agreement with the results obtained at the electrochemical cell depicted above.

Assuming that the electrochemical efficiency is the theoretical efficiency (0.97) × cell potential/reversible cell potential (V_{cell}), and the voltage efficiency is V_{cell}/1.144 [63], the electrochemical fuel cell efficiency for the MEAs in Fig. 7 can be estimated in the region relevant for the DEFC operation, that is, before the peak power density. Thus, at representative current of 10 mA mg_{Pt}^{-1}, the electrochemical efficiencies were 40.2, 19.0, 18.1, and 12.6% for MEAs containing Pt_1Sn_1/C, Pt_3Sn_1/C, Pt_1Sn_1/CNF, and Pt_3Sn_1/CNF catalysts, respectively.

The differences between the performance of the catalysts in the single DEFC and in the three-electrode cell experiments could be explained by the different temperature (i.e. electrode preparation and working conditions), so in spite of the different conditions, the results of the two types of catalyst supports are consistent: catalyst

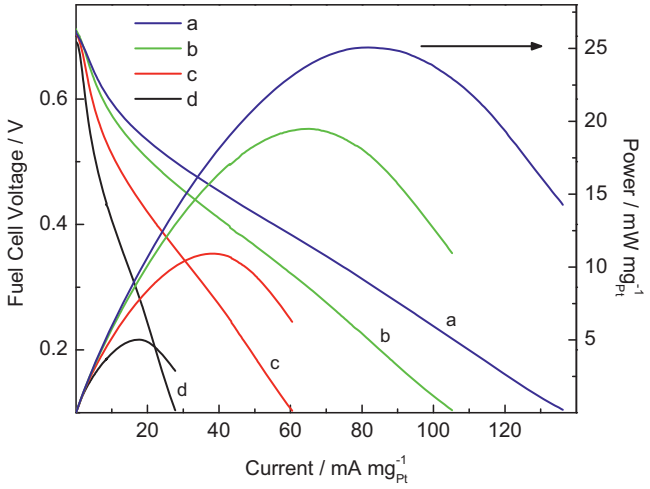

Fig. 8. Voltage vs. current density and power density vs. current density curves for DEFC. Influence of working temperature on fuel cell performance. MEA made of Pt_1Sn_1/C (anode) and 2.0 mg_{Pt} cm^{-2} Pt/C (cathode). Temperature: (a) 90.0, (b) 80.0; (c) 60.0, and (d) 40.0 °C. Anode fed with 2.0 M CH_3CH_2OH at 1.5 mL min^{-1}; cathode fed with dry O_2 at 50 mL min^{-1}.

supported on carbon black have better activity for the EOR than those supported on carbon nanofibers. In addition, the difference between the curves is maintained in the whole current interval. This means that the difference is due only to the nature of the catalysts at the anode, since Pt/C catalyst with the same loading was coated on the cathode side, and depends strongly on the material support.

The effect of temperature on the cell performance was studied with the catalyst that develops the best performance, which is Pt_1Sn_1/C. Fig. 8 clearly shows that raising the temperature greatly increased the fuel cell performance, from a maximum power density of 5.02 mW cm^{-2} at 40 °C, to 25.1 mW cm^{-2} at 90 °C, that is, five times higher. This fact confirms the difficulty to oxidize ethanol at low temperatures, and the necessity to increase the working temperature to enhance the electrode kinetics, and thus, the DEFC performance.

4. Conclusions

In the present work, the activity toward ethanol electrooxidation of PtSn catalysts supported on a commercial carbon black (Vulcan XC72R) and carbon nanofibers chemically treated was investigated. A series of PtSn catalysts with different Pt:Sn atomic ratio (1:1 and 3:1) were synthesized by using the formic acid method. The physicochemical characteristics showed that the mean particle size of all catalysts was approximately 4 nm and there was good dispersion over carbon catalyst supports. XRD analysis indicates the presence of SnO_2 species at all materials and higher amount of Pt_3Sn_1 crystallite phase in the Pt_1Sn_1 catalyst respect to the Pt_3Sn_1 sample, the last having an important effect on the whole catalytic behavior.

Based on the electrochemical results, the addition of Sn and the content of Pt_3Sn_1 crystallite phase strongly improve the platinum activity toward carbon monoxide and ethanol electrooxidation. Furthermore, there is a distinctive effect depending on the Sn content and the catalyst support used. Specifically, catalysts supported on carbon nanofibers with Pt:Sn 1:1 atomic ratio and high content in Pt_3Sn_1 crystallite phase displayed the highest activity toward CO_{ad} electrooxidation. However, greatest performance for ethanol elecctrooxidation in a DEFC, in terms of produced power, was obtained for Pt_1Sn_1 supported on Vulcan XC-72R, which displays worse behavior for CO stripping. Consequently, as the best catalyst for CO_{ad} electrooxidation is not the best for the EOR, it is suggested that the delivered current for EOR is mainly produced by side-products such as acetaldehyde and acetic acid. Accordingly, an important effect of the temperature was observed toward the EOR for the measurements achieved at single DEFC, confirming the importance of this parameter for the cleavage of C—C bond thus increasing the current and power densities under operational conditions in a fuel cell.

Acknowledgments

The authors gratefully acknowledge financial support given by the Spanish MINECO under projects CTQ2011-28913-C02-01 y 02 and Fundación Cajacanarias under project BIOGRAF. J.C.C. is indebted to the Alßan Program for the predoctoral fellowship No. E07D403742CO.

References

[1] U.B. Demirci, J. Power Sources 169 (2007) 239–246.
[2] C. Lamy, A. Lima, V. LeRhun, F. Delime, C. Coutanceau, J.M. Léger, J. Power Sources 105 (2002) 283–296.
[3] W.J. Zhou, B. Zhou, W.Z. Li, Z.H. Zhou, S.Q. Song, G.Q. Sun, Q. Xin, S. Douvartzides, M. Goula, P. Tsiakaras, J. Power Sources 126 (2004) 16–22.
[4] F. Vigier, C. Coutanceau, A. Perrard, E.M. Belgsir, C. Lamy, J. Appl. Electrochem. 34 (2004) 439–446.
[5] F. Vigier, C. Rousseau, C. Coutanceau, J.M. Léger, C. Lamy, Top. Catal. 40 (2006) 111–121.
[6] F.J. Rodríguez-Varela, O. Savadogo, J. Electrochem. Soc. 155 (2008) B618–B624.
[7] S. Song, V. Maragou, P. Tsiakaras, J. Fuel Cell Sci. Technol. 4 (2007) 203–209.
[8] K. Taneda, Y. Yamazaki, Electrochim. Acta 52 (2006) 1627–1631.
[9] Y. Paik, S.S. Kim, O.H. Han, Electrochem. Commun. 11 (2009) 302–304.
[10] D.D. James, D.V. Bennett, G. Li, A. Ghumman, R.J. Helleur, P.G. Pickup, Electrochem. Commun. 11 (2009) 1877–1880.
[11] A. Oliveira Neto, M.J. Giz, J. Perez, E.A. Ticianelli, E.R. Gonzalez, J. Electrochem. Soc. 149 (2002) A272–A279.
[12] G. García, N. Tsiouvaras, E. Pastor, M.A. Peña, J.L.G. Fierro, M.V. Martínez-Huerta, Int. J. Hydrogen Energy 37 (2012) 7131–7142.
[13] H. Hitmi, E.M. Belgsir, J.M. Léger, C. Lamy, R.O. Lezna, Electrochim. Acta 39 (1994) 407–415.
[14] S.L. Blair, W.L.S. Law, in: H. Liu, J. Zhang (Eds.), Electrocatalysis of Direct Methanol Fuel Cells, Wiley-VCH Verlag GmbH & Co. kGaA, Weinheim, 2009, p. 545.
[15] E. Antolini, J. Power Sources 170 (2007) 1–12.
[16] S. García-Rodríguez, M.A. Peña, J.L.G. Fierro, S. Rojas, J. Power Sources 195 (2010) 5564–5572.
[17] F.H.B. Lima, E.R. Gonzalez, Electrochim. Acta 53 (2008) 2963–2971.
[18] A.O. Neto, R.R. Dias, M.M. Tusi, M. Linardi, E.V. Spinacé, J. Power Sources 166 (2007) 87–91.
[19] W.J. Zhou, W.Z. Li, S.Q. Song, Z.H. Zhou, L.H. Jiang, G.Q. Sun, Q. Xin, K. Poulianitis, S. Kontou, P. Tsiakaras, J. Power Sources 131 (2004) 217–223.
[20] A. Kowal, S.L. Gojković, K.S. Lee, P. Olszewski, Y.E. Sung, Electrochem. Commun. 11 (2009) 724–727.
[21] A.S. Aricò, V. Antonucci, P.L. Antonucci, in: A. Wieckowski, E.R. Savinova, C.G. Vayenas (Eds.), Catalysis and Electrocatalysis at Nanoparticle Surface, Marcel Dekker, Inc., New York, 2003, p. 613.
[22] A.L. Dicks, J. Power Sources 156 (2006) 128–141.
[23] X. Yang, J. Zheng, M. Zhen, X. Meng, F. Jiang, T. Wang, C. Shu, L. Jiang, C. Wang, Appl. Catal. B-Environ. 121–122 (2012) 57–64.
[24] X. Jin, B. He, J. Miao, J. Yuan, Q. Zhang, L. Niu, Carbon 50 (2012) 3083–3091.
[25] W. Li, C. Liang, W. Zhou, J. Qiu, Z. Zhou, G. Sun, Q. Xin, J. Phys. Chem. B 107 (2003) 6292–6299.
[26] Y. Cheng, S.P. Jiang, Electrochim. Acta 99 (2013) 124–132.
[27] H. Tang, J.H. Chen, Z.P. Huang, D.Z. Wang, Z.F. Ren, L.H. Nie, Y.F. Kuang, S.Z. Yao, Carbon 42 (2004) 191–197.
[28] D. Sebastián, J.C. Calderón, J.A. González-Expósito, E. Pastor, M.V. Martínez-Huerta, I. Suelves, R. Moliner, M.J. Lázaro, Int. J. Hydrogen Energy 35 (2010) 9934–9942.
[29] D. Sebastián, I. Suelves, E. Pastor, R. Moliner, M.J. Lázaro, Appl. Catal. B-Environ. 132–133 (2013) 13–21.
[30] Y.C. Liu, X.P. Qiu, Y.Q. Huang, W.T. Zhu, Carbon 40 (2002) 2375–2380.
[31] Y.C. Liu, X.P. Qiu, Y.Q. Huang, W.T. Zhu, J. Power Sources 111 (2002) 160–164.
[32] R. Yang, X. Qiu, H. Zhang, J. Li, W. Zhu, Z. Wang, X. Huang, L. Chen, Carbon 43 (2005) 11–16.
[33] J.C. Calderón, N. Mahata, M.F.R. Pereira, J.L. Figueiredo, V.R. Fernandes, C.M. Rangel, L. Calvillo, M.J. Lázaro, E. Pastor, Int. J. Hydrogen Energy 37 (2012) 7200–7211.
[34] N. Job, J. Marie, S. Lambert, S. Berthon-Fabry, P. Achard, Energy Convers. Manage. 49 (2008) 2461–2470.
[35] Y. Guo, Y. Zheng, M. Huang, Electrochim. Acta 53 (2008) 3102–3108.
[36] J.C. Calderón, G. García, L. Calvillo, J.L. Rodríguez, M.J. Lázaro, E. Pastor, Appl. Catal. B-Environ. (2014), http://dx.doi.org/10.1016/j.apcatb.2014.10.077.
[37] S. Kang, S. Lim, D.H. Peck, S.K. Kim, D.H. Jung, S.H. Hong, H.G. Jung, Y. Shul, Int. J. Hydrogen Energy 37 (2012) 4685–4693.
[38] A. Santasalo-Aarnio, M. Borghei, I.V. Anoshkin, A.G. Nasibulin, E.I. Kauppinen, V. Ruiz, T. Kallio, Int. J. Hydrogen Energy 37 (2012) 3415–3424.
[39] L. Calvillo, M.J. Lázaro, I. Suelves, Y. Echegoyen, E.G. Bordejé, R. Moliner, J. Nanosci. Nanotechnol. 9 (2009) 4164–4169.
[40] L. Calvillo, V. Celorrio, R. Moliner, M.J. Lázaro, Mater. Chem. Phys. 127 (2011) 335–341.
[41] L. Calvillo, V. Celorrio, R. Moliner, A.B. Garcia, I. Caméan, M.J. Lazaro, Electrochim. Acta 102 (2013) 19–27.
[42] W.J. Zhou, S.Q. Song, W.Z. Li, Z.H. Zhou, G.Q. Sun, Q. Xin, S. Douvartzides, P. Tsiakaras, J. Power Sources 140 (2005) 50–58.
[43] C. Lamy, S. Rousseau, E.M. Belgsir, C. Coutanceau, J.M. Léger, Electrochim. Acta 49 (2004) 3901–3908.
[44] Z. Liu, B. Guo, L. Hong, T.H. Lim, Electrochem. Commun. 8 (2006) 83–90.
[45] P. Bommersbach, M. Mohamedi, D. Guay, J. Electrochem. Soc. 154 (2007) B876–B882.
[46] F.L.S. Purgato, P. Olivi, J.M. Léger, A.R. de Andrade, G. Tremiliosi-Filho, E.R. Gonzalez, C. Lamy, K.B. Kokoh, J. Electroanal. Chem. 628 (2009) 81–89.
[47] (a) I. Suelves, M.J. Lázaro, R. Moliner, B.M. Corbella, J.M. Palacios, Int. J. Hydrogen Energy 30 (2005) 1555–1567;
(b) I. Suelves, M.J. Lázaro, R. Moliner, Y. Echegoyen, J.M. Palacios, Catal. Today 116 (2006) 271–280.
[48] E.R. Gonzalez, E.A. Ticianelli, A.L.N. Pinheiro, J. Perez, INPI-SP, Vol. 00321, Brazil, 1997.
[49] B.E. Warren, X-ray Diffraction, Addison-Wesley Pub. Co, Reading, MA, 1969.
[50] Y.P. Mascarenhas, J.M.V. Pinheiro, Programa para Calculo de Parametro de Rede pelo Metodo de Minimos Quadrados, SBPC, Brazil, 1985.

[51] F. Alcaide, G. Álvarez, O. Miguel, M.J. Lázaro, R. Moliner, A. López-Cudero, J. Solla-Gullón, E. Herrero, A. Aldaz, Electrochem. Commun. 11 (2009) 1081–1084.
[52] L. Colmenares, H. Wang, Z. Jusys, L. Jiang, S. Yan, G.Q. Sun, R.J. Behm, Electrochim. Acta 52 (2006) 221–233.
[53] J.O.M. Bockris, S.U.M. Khan, Surface Electrochemistry: A Molecular Level Approach, Plenum Press, New York, 1993, pp. 4.
[54] G. García, M.T.M. Koper, Chem. Phys. Chem. 12 (2011) 2064–2072.
[55] O. Guillén-Villafuerte, G. García, A. Orive, B. Anula, A. Creus, E. Pastor, Electrocatalysis 2 (2011) 231–241.
[56] T.J. Schmidt, M. Noeske, H.A. Gasteiger, R.J. Behm, P. Britz, H. Bönnemann, J. Electrochem. Soc. 145 (1998) 925–931.
[57] D.-H. Lim, D.-H. Choi, W.-D. Lee, H.-I. Lee, Appl. Catal. B-Environ. 89 (2009) 484–493.
[58] E. Antolini, E.R. Gonzalez, Electrochim. Acta 56 (2010) 1–14.
[59] E.V. Spinacé, M. Linardi, A.O. Neto, Electrochem. Commun. 7 (2005) 365–369.
[60] W.J. Zhou, S.Q. Song, W.Z. Li, G.Q. Sun, Q. Xin, S. Kontou, K. Poulianitis, P. Tsiakaras, Solid State Ionics 175 (2004) 797–803.
[61] J. Ribeiro, D.M. dos Anjos, K.B. Kokoh, C. Coutanceau, J.M. Léger, P. Olivi, A.R. de Andrade, G. Tremiliosi-Filho, Electrochim. Acta 52 (2007) 6997–7006.
[62] K. Nam, K. Seongyop, S.-K. Kim, S.-H. Yoon, D.-H. Jung, Int. J. Hydrogen Energy 37 (2012) 4619–4626.
[63] S. Rousseau, C. Coutanceau, C. Lamy, J.-M. Léger, J. Power Sources 158 (2006) 18–24.